Probing the Mechanism of the Hamster Mitochondrial Folate Transporter by Mutagenesis and Homology Modeling

Erin Perchiniak,‡ Scott A. Lawrence,‡ Shane Kasten,‡ B. Ann Woodard, Shirley M. Taylor, and Richard G. Moran*

Department of Pharmacology and Toxicology and Massey Cancer Center, Virginia Commonwealth University, Richmond, Virginia 23298

Received October 21, 2006; Revised Manuscript Received December 1, 2006

ABSTRACT: The mitochondrial folate transporter (MFT) was previously identified in human and hamster cells. Sequence homology of this protein with the inner mitochondrial membrane transporters suggested a domain structure in which the N- and C-termini of the protein are located on the mitochondrial intermembrane-facing surface, with six membrane-spanning regions interspersed by two intermembrane loops and three matrix-facing loops. We now report the functional significance of insertion of the c-*myc* epitope into the intermembrane loops and of a series of site-directed mutations at hamster MFT residues highly conserved in orthologues. Insertional mutagenesis in the first predicted intermembrane loop eliminated MFT function, but the introduction of a c-*myc* peptide into the second loop was without effect. Most of the hamster MFT residues studied by site-directed mutagenesis were remarkably resilient to these mutations, except for R249A and G192E, both of which eliminated folate transport activity. Homology modeling, using the crystal structure of the bovine ADP/ATP carrier (AAC) as a scaffold, suggested a similar three-dimensional structure for the MFT and the AAC. An ion-pair interaction in the AAC thought to be central to the mechanism of membrane penetration by ADP is predicted by this homology model to be replaced by a π−cation interaction in MFT orthologues and probably also in other members of the family bearing the P(I/L)W motif. This model suggests that the MFT R249A and G192E mutations both modify the base of a basket-shaped structure that appears to constitute a trap door for the flux of folates into the mitochondrial matrix.

Folate metabolism in mammalian cells is distributed between the cytosolic and mitochondrial compartments, and the shuttling of folates and one-carbon units through the mitochondrial membrane is essential for cell survival (*1*−*6*). In the absence of mitochondrial folate metabolism, either because of mutations that affect folate transport into the organelle (*7*) or genetic manipulations that allow folylpolyglutamate synthetase activity only in the cytosol and not in mitochondria (*3*, *8*), mammalian cells require a supply of glycine in the medium. In previous studies (*7*), we isolated a cDNA that encoded a mitochondrial inner membrane protein subsequently (*9*) identified as the mitochondrial transport protein for folates. This mitochondrial folate transport (MFT)[1] protein reinstated the accumulation of folates within the mitochondrial matrix in a CHO mutant cell line, the glyB cell, that was deficient in this process (*7*), and the genetic basis of the glyB auxotrophic phenotype was shown to be a point mutation in the *mft* (*9*).

The MFT protein has the defining characteristics of the inner mitochondrial membrane transport carriers (MCPs), proteins encoded by a moderate size gene family estimated by in silico experiments to have 35 members in yeast (*10*). Analysis of the human genome sequence has predicted that there are 75 members of this family in man, of which the function of 21 has been assigned (*11*). The MCP family members have 300−330 amino acids and six predicted transmembrane domains (*12*). Previous studies on members of this family have documented that the N- and C-termini of these proteins are located on the outside of the inner mitochondrial membrane, so that the six transmembrane domains (TMDs) result in two loops on the intermembrane space side and three on the matrix side of the inner mitochondrial membrane (*13*−*15*). Members of the MCP family are easily recognized by their tripartite repeat motifs and a defining signature peptide [PX(D/E)XX(R)] placed at the C-terminus of the first, third, and fifth predicted membrane-spanning regions (*16*). Elegant crystallographic experiments by Brandolin and colleagues (*17*) on the prototypical member of this family, the bovine ADP/ATP carrier (AAC), revealed a monomeric unit containing six transmembrane helices forming a mitochondrial membrane-spanning cone with an interior cavity that appears to be contiguous with the aqueous phase of the intermembrane space. The opening of this apparent transport channel was as large as 20 Å, and there were a series of hydrophilic surfaces on the walls of the channel, whereas the more hydrophobic regions of the transmembrane domains were oriented toward the lipid phase of the membrane (PDB codes: 1okc and 2c3e). A natural product inhibitor car-

* To whom correspondence should be addressed. Phone: 804-828-5783. Fax: 804-827-0810. E-mail: rmoran@hsc.vcu.edu.

‡ These authors contributed equally to this work.

[1] Abbreviations: MFT, mitochondrial folate transporter; AAC, ADP/ATP carrier; PCR, polymerase chain reaction; MCP, mitochondrial carrier protein; TMD, transmembrane domain; IM, intermembrane loop; SD, standard deviation; 5-fTHF, 5-formyltetrahydrofolate.

10.1021/bi062191+ CCC: $37.00
Published on Web 01/20/2007

boxyatractyloside (CATR) cocrystallized with the AAC monomer was oriented deep within the cavity, fixed in place by interactions with several basic residues on a shelf in the structure, located two-thirds of the distance through the membrane. It has been proposed (*17*) that loading of substrate deep in the cavity causes a shift of the helices at the base of transmembrane domains (TMDs) 1, 3, and 5, removing the barrier preventing substrate entry into the mitochondrial matrix. The sequence differences among the individual MCP family members that cause the substrate acceptance patterns and the degree to which these transporters have a common mechanism are of current interest.

In this paper, we investigate the mechanism of folate transport into mitochondria using mutagenesis and homology modeling. The mutations were created in an N-terminal c-*myc*-tagged hamster *mft* cDNA, which allows effects on transport to be distinguished from trafficking defects. Interruption of one of the intermembrane loops with the c-*myc* epitope eliminated transport by this protein. Two point mutations were also identified that prevented transport, and homology modeling suggested that both mutations interfered with the "trap-door" mechanism of this carrier.

EXPERIMENTAL PROCEDURES

Materials. GlyB cells, a CHO-K1 derivative, were generously provided by Professor Lawrence Chasin from Cornell University (*18*, *19*). The cells were negative for mycoplasma and were routinely grown in α-MEM supplemented with 10% fetal calf serum (FCS).

Construction of myc-Tagged mft Constructs. The CHO MFT cDNA (*7*) cloned into pcDNA 3.1(−) was used as template to insert the *c-myc* epitope into the N- and C-termini and intermembrane loops IM1 and IM2. The C-terminal *c-myc*-tagged cDNA was generated by amplifying the open reading frame with primers that added an *Eco*RV site at the 5′ end (sense primer: 5′-cccgatatcAGTGTCGCCACG-GTGGC-3′) (coding sequence is in upper case) and an *Xho*I site at the 3′ end (antisense primer: 5′-cccctcgagCTTTTCTC-GAAGGCCACAC-3′). The resulting PCR product lacked sequence encoding the three C-terminal amino acids. The restriction digested and purified PCR product was cloned into pcDNA3.1/myc-HIS A, which carries the c-*myc* tag 3′ to the multiple cloning site. To insert the c-*myc* tag at the N-terminus of CHO and glyB MFT cDNAs, these sequences were first modified by PCR to delete the start methionine and add restriction endonuclease sites for *Xho*I and *Sac*II at the 5′ end (sense primer: 5′-cccctcgagccgcggACAGGC-CAGGGG-3′) and a *Hin*dIII site at the 3′ end (antisense primer: 5′-gggaagcttCTCAGGCAGATACGCTGG-3′) for subsequent cloning steps. The products were recloned into pcDNA3.1(−) and sequenced. The DNA sequence encoding the 10 amino acid c-*myc* epitope, EQKLISEEDL, was used to design a pair of complementary oligonucleotides, flanked at both the 5′ and 3′ ends by the recognition site for *Sac*II, and encoding a Kozak's sequence and start methionine (sense primer, 5′-tccccgcgggccgccaccatggaacaaaaactcatctcagaagag-gatctgcggcgggga-3′; antisense primer, 5′-tccccgcggcagatc-ctcttctgagatgagtttttgttccatggtggcggcccgcgggga-3′). Five micrograms of each oligonucleotide was combined in 10 μL, the mixture was incubated at 90 °C for 4 min and 70 °C for 10 min, and then allowed to slowly cool to room temperature. The double-stranded oligonucleotide was digested with *Sac*II, gel purified, and cloned into the *Sac*II-modified MFT plasmids.

Insertion of the c-*myc* tag into IM1 and IM2 was achieved using PCR to insert unique restriction sites into each domain. *Sac*II was inserted into IM1 immediately N-terminal to the first amino acid of TM3, between amino acids E122 and Y123, and *Bam*HI was inserted midway into IM2 between amino acids I214 and N215. Briefly, the CHO MFT cDNA was amplified in two fragments for each construct from 66 base pairs upstream of the start ATG to the c-*myc* insertion site and from the insertion site to 24 bases downstream of the stop codon. *Xho*I and *Hin*dIII restriction sites were added to the 5′ and 3′ ends, respectively, for reinsertion into pcDNA3.1(−). PCR fragments were digested with the appropriate restriction endonucleases, gel purified, and ligated into the *Xho*I and *Hin*dIII digested vector. PCR reactions contained 0.2 μg of the CHO *mft* cDNA as template (*9*), 1 unit of *Taq* polymerase, and 1 unit of *Pfu* polymerase (Stratagene) in a total reaction volume of 25 μL. The double-stranded c-*myc* oligonucleotide, flanked by *Sac*II or *Bam*HI restriction sites, was then inserted into the modified MFT vectors. The direction of insertion of the c-*myc* tag was verified by sequence analysis, and the correctly modified clones were completely sequenced using vector-specific primers. The peptide sequences inserted into the intermembrane loops were (bold type) IM1, PLE^{122}**prEQKLISEEDLpr**Y^{123}LVS, and IM2, KHI^{214}**gsEQKLISEEDLgs**N^{215}RLP, with the residues added by the new restriction sites in lower case and the *myc* tag in upper case.

Site-Directed Mutagenesis. Ten site-directed mutants were made within the ORF of the *mft* using overlap extension PCR (*20*). For each mutant, two separate first-round PCR reactions, each including a vector-specific primer and a gene-specific primer which introduced the mutation, were performed using a mixture of *Taq* (2 units) and *Pfu* (0.5 unit) polymerases. For each mutation, the two PCR products were gel-purified, and 50 ng of each first-round PCR product was combined in a second round of PCR which used the two flanking, vector-specific primers to amplify the mutated *mft* cDNA as one fragment. After each mutation was added to the ORF of the *mft*, each 1148 bp fragment was subcloned into pcDNA3.1(−), using *Xho*I and *Hin*dIII restriction sites that had been added to the CHO *mft* in the PCR primers at the 5′ and 3′ ends, respectively. All clones were sequenced prior to use.

Transfection Studies. Actively growing glyB cells maintained in α-MEM (Invitrogen) supplemented with 10% FCS were plated at a density of 1×10^5 cells on 100 mm dishes. After 24 h, 5 μg of plasmid DNA was added to each plate as a calcium phosphate precipitate as previously described (*9*). For each construct, triplicate plates were transfected in each experiment, and the reported data represent the results of three to six experiments, except when noted. After 30 min at room temperature, 9 mL of complete medium was added to each plate, the plates were incubated at 37 °C overnight and then briefly shocked with Me_2SO the following day, and nonselective medium was added. Cells were placed under single selection [G418 (1 mg/mL), α-MEM with glycine and containing 10% dialyzed serum] or double selection [G418 (1 mg/mL), glycine-free α-MEM containing

dialyzed serum] 24 h after Me_2SO treatment. Plates were fed daily, and colonies emerging 10 days after transfection were fixed, stained, and manually counted.

Uptake of [^{3}H]-(6S)-5-Formyltetrahydrofolate (^{3}H-5-fTHF). Stably transfected colonies were isolated from plates of glyB cells after calcium phosphate transfections with mutant MFT cDNAs, and the colonies were individually mass-cultured. Equal numbers of cells from 10 such cultures for each mutation were pooled, and the mutant pools were used for transport assays within three passages. Pooled colony cultures were grown in α-MEM medium with deoxyribonucleosides and ribonucleosides supplemented with 10% FBS, and cells were detached with trypsin/EDTA, resuspended in α-MEM, equilibrated with 5% CO_2, and then placed in a shaker at 37 °C for 2 h to allow recovery from trypsin. Cells were pelleted and resuspended in RPMI 1640 medium without folic acid supplemented with 20 mM HEPES/10 mM MOPS. Aliquots of the cell suspension (0.25 mL) containing ≈15 million cells were distributed into tubes and preequilibrated for 5 min at 37 °C. Uptake was initiated by the timed addition of 0.25 mL of RPMI 1640 medium without serum or folate, containing HEPES/MOPS and 2 μM ^{3}H-5-fTHF at 10 μCi/mL (≈3200 cpm/pmol). Triplicate tubes were exposed to ^{3}H-5-fTHF at each point. Uptake was stopped by the timed addition of 10 mL of ice-cold PBS, and cells were pelleted and washed two additional times in 10 mL of cold PBS. Cell pellets were resuspended in 1.8 mL of homogenization solution (0.25 M sucrose and 1 mM EDTA, pH 6.8), and mitochondrial and cytosolic fractions were prepared by differential centrifugation as previously reported (*7*). Briefly, cells were lysed with 30 strokes of a tight-fitting Dounce homogenizer, and unbroken cells and nuclei were harvested by centrifugation. These initial pellets were dounced again, and the pellets from the second homogenization were washed once with homogenization buffer. The three supernatant fractions were combined, residual unbroken cells/nuclei were removed from this mixture by centrifugation at 900*g* for 5 min, and the supernatant was then centrifuged at 10000*g* for 15 min to separate mitochondrial and cytosolic fractions. The pelleted fractions were dissolved in NaOH and then acidified with HCl. Radioactivity in the subcellular fractions was determined by scintillation counting.

Mitochondrial Isolation. Plasmids encoding MFT variants were transfected into three 100 mm plates of glyB cells as above, and cells from colonies formed after 10 days of double selection were pooled and replated into 150 mm dishes. For transfectants which were not viable under double selection, e.g., R249A, transfectants were pooled and expanded under single selection. The pooled transfectants were expanded, and mitochondria were isolated using a mitochondrial isolation kit for mammalian cells (Pierce). The cytosolic fraction was concentrated on an YM-30 Centricon filtration device (Amicon) to a protein concentration of 3 mg/mL of protein. The mitochondrial pellet was resuspended in 25 μL of sample buffer (62.5 mM Tris, pH 6.8, 5% glycerol, 2% SDS, 5% 2-mercaptoethanol). Protein concentrations were determined using the modified Bradford assay (Bio-Rad) according to the manufacturer's directions.

Western Blotting. Forty micrograms of subcellular protein fractions was separated on a 7.5% polyacrylamide gel and transferred to a PVDF membrane using a semidry transfer apparatus for 1.5 h at 40 mA. Nonspecific protein binding was blocked for 1 h at room temperature in Blotto (0.01 M Tris, pH 7.4, 0.15 M NaCl, 5% nonfat dry milk, 0.1% Tween 20). The blocked membranes were rinsed three times for 5 min in TBS-T (0.5 M Tris, pH 7.5, 0.14 M NaCl, 2.7 mM KCl, 0.05% Tween 20) and then incubated overnight at 4 °C with primary antibody diluted in 5% nonfat dry milk and TBS-T. Rabbit anti-c-*myc* antibody (Sigma C3956) was used at 1.0 μg/mL, goat anti-lactate dehydrogenase polyclonal (Abcam ab7639) at a 1:2500 dilution, and rabbit anti-porin (EMD Biosciences PC548) at 1:2500. After incubation overnight in primary antibody, the blots were rinsed three times for 5 min in TBS-T and then incubated in secondary antibody (at 1200−2500) conjugated to horseradish peroxidase (Pierce), diluted in 5% milk and TBS-T, for 1 h at room temperature. The membranes were again rinsed three times for 5 min in TBS-T, and protein complexes were detected by enhanced chemiluminescence using the SuperSignal West Pico chemiluminescent substrate kit (Pierce).

Homology Modeling. Two homology models of the MFT structure were constructed. The first was generated by submitting the *Cricetulus griseus* MFT primary sequence (GenBank accession number AY611603) to the ESyPred3D server with the coordinates of the bovine mitochondrial ATP/ADP carrier (bAAC) structure (PDB code: 1okc, chain A) selected as a threading template (*21*). The modeling package MODELLER was employed by ESyPred3D to estimate the 3D structure for the hamster MFT. The optimized model consisted of a continuous polypeptide chain comprising residues 17−303 of the hamster protein. The ESyPred3D homology model was inspected for conserved region-specific alignment reliability; then the 3D structure was assessed by generating a pairwise superposition of the ESyPred3D model and the bAAC template using the Swiss-PdbViewer program, followed by RMSD calculations using only C_∞ spatial arrangements for all residues (*22*). The algorithms Verify3D profiles (*23*) and ProsaII *Z*-scores (*24*) were used to evaluate the reliability of the predicted ESyPred3D model structure. The second homology model was generated using Tripos Sybyl Composer v7.1. A user-defined, template database was created containing the 3D coordinates of two crystallizations of bovine AAC (PDB codes: 1okc and 2c3e). Predicted structural similarities and conserved sequences were aligned, followed by the generation of a 3D MFT model. This Sybyl model was subjected to side chain placement optimization using the SCWRL 3.0 program (*25*).

RESULTS

N- and C-Terminal c-myc Tags Do Not Prevent MFT Trafficking and Mitochondrial Folate Transport. Two observations convinced us that the *mft* gene product facilitates mitochondrial folate transport: (1) a retrovirus containing a human *mft* gene complemented both the deficient mitochondrial folate pool of glyB cells and the inability of these cells to grow in the absence of glycine (*7*, *18*, *19*, *26*), and (2) the CHO-derived glyB cell had an inactivating mutation (G192E) in the *mft* gene (*9*). The c-*myc* fusion tag was added to the CHO *mft* cDNA, and the function of the N- or C-terminal tagged proteins was determined by stably transfecting the cDNAs into glyB cells and assessing the survival of transfectants in medium without glycine (Figure 1). Consistent with previous studies (*7*, *9*), glyB cells transfected

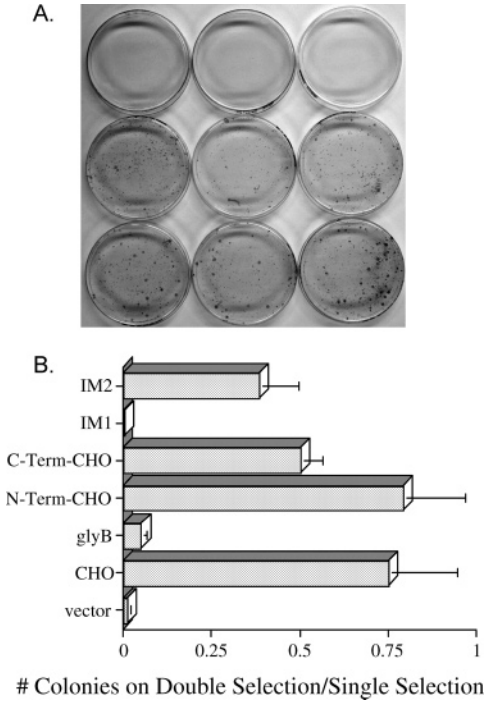

FIGURE 1: MFT function is altered by insertional mutagenesis of intermembrane loop 1. (A) Survival of glyB cells stably transfected with modified CHO *mft* cDNAs. The top two rows of plates were fed glycine-depleted medium containing G418 to test folate transport function in proteins encoded by modified CHO *mft* cDNAs. The cDNAs transfected were as follows: top row (left to right), pcDNA3.1 (−), glyB *mft*, and IM1 *c-myc*-tagged CHO *mft*; middle row (left to right), N-term *c-myc*-tagged CHO *mft*, C-term *c-myc*-tagged CHO *mft*, and IM2 *c-myc*-tagged *mft*. The bottom row of plates was transfected with (left to right) N-term *c-myc*-tagged CHO *mft*, C-term *c-myc*-tagged CHO *mft*, and IM2 *c-myc*-tagged *mft* and were fed with medium containing glycine and G418 as transfection controls. Single selection plates were similar for all conditions. (B) Fraction of transfected cells that formed colonies in the absence of glycine. The data are expressed as a ratio of colony formation under double selection (G418 − glycine) to colonies formed under single selection (G418 + glycine), averaged over two to six experiments, with three dishes per experiment.

with the wild-type hamster *mft* cDNA did not require glycine, whereas glyB cells transfected with the mutant glyB *mft* cDNA, or the vector alone, did not survive in medium lacking glycine. Stable transfectants of both the N- and C-terminal c-*myc*-tagged CHO MFT constructs survived in the absence of glycine, and hence, these epitope tags did not interfere with mitochondrial folate transport (Figure 1). This allowed us to follow the subcellular distribution of epitope-tagged proteins derived from c-*myc*-tagged constructs. The N-terminal tagged MFT construct was used as a mutagenesis scaffold since transfection of the C-terminal tagged MFT resulted in lower colony-forming efficiency (Figure 1).

The glyB (G192E) Point Mutation Does Not Alter Mitochondrial Targeting of the MFT Protein. The c-*myc* fusion tag was added to the N-terminus of the nonfunctional G192E glyB MFT protein. Mitochondrial and cytosolic proteins from glyB cells stably transfected with the *myc*-tagged G192E MFT cDNA were subjected to Western blot analysis using a c-*myc* antibody. Protein from stably transfected glyB cells expressing the c-*myc*-tagged CHO MFT was used as a control for mitochondrial localization, and blots were reprobed with an antibody against the voltage-dependent anion

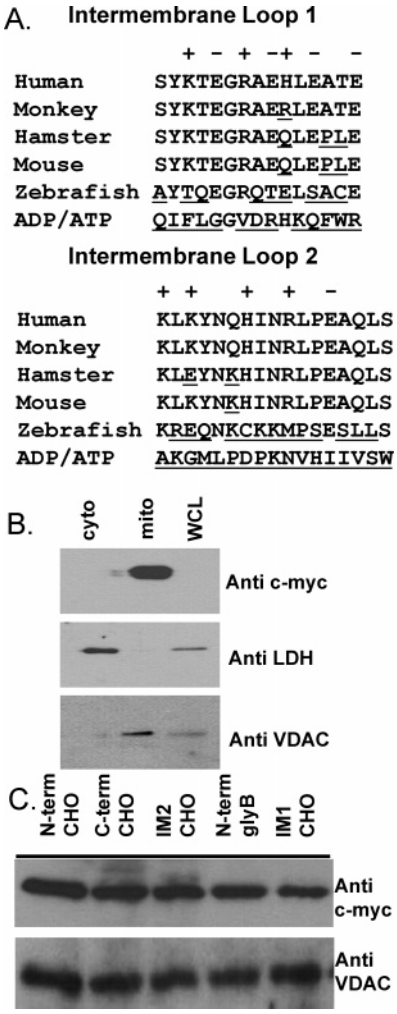

FIGURE 2: Mitochondrial localization of MFT is not disrupted by insertion of the c-*myc* tag. (A) Sequence alignment of the two intermembrane loop regions from MFT orthologues and from the bovine AAC. Underlined residues differ from the human MFT sequence. The charge state of side chains in the human sequence is shown above the sequence comparison. (B) Detection of the c-*myc* antigen in the unfractionated cell lysates (WCL) and in the cytosolic (cyto) and mitochondrial (mito) fractions of glyB cells transfected with the N-terminal c-*myc*-tagged CHO *mft* cDNA and of antigens for mitochondrial (VDAC) and cytosolic (LDH) proteins. The c-*myc*-tagged CHO MFT protein was only detected in the mitochondrial fraction. (C) Detection of MFT proteins in the mitochondrial fractions of glyB cells stably transfected with modified CHO *mft* cDNAs. Forty micrograms of mitochondrial protein from each transfectant was resolved, blotted, and probed with antibodies to c-*myc* and VDAC. All tagged MFT proteins were detected only in the mitochondria.

channel (VDAC) protein, a mitochondrial marker (*27*), as a loading control. The c-*myc* antigen of these constructs was found in the mitochondrial but not the cytosolic fraction at protein loads up to 40 μg per lane, as shown for cells transfected with the N-terminal c-*myc*-tagged CHO cDNA (Figure 2B). The c-*myc*-tagged glyB MFT clearly localized to the mitochondria, ruling out the possibilities that the glyB mutation caused poor mitochondrial targeting or instability of the mutant protein. We concluded that the G192E mutation interfered with the mechanism of transport catalyzed by the MFT.

Insertion of a Peptide into Intermembrane Loop 1 Blocks Function. The two small loop regions of the MFT protein predicted to face the intermembrane space were very well

Table 1: Residues at Positions Chosen for Mutagenesis in MFT Orthologues, the Putative Chloroplast Folate Transporter, and the ADP/ATP Exhanger (AAC)[a]

MFT							
hamster	human	monkey	mouse	zebrafish	At-FT1	predicted domain	AAC
R19	R	R	R	K	A	N-terminus/TMD1 interface	L
H41	H	H	H	H	H	TMD1	A
S95	S	S	S	S	S	TMD2	T
R114	R	R	R	R	D	intermembrane loop 1	V
E129	E	E	E	E	E	TMD3	A
K184	K	K	K	K	R	TMD4	Q
E209	K	K	K	E	K	intermembrane loop 2	M
E219	E	E	E	E	D	intermembrane loop 2	P
R249	R	R	R	R	R	TMD5	R
H256	H	H	H	H	P	matrix loop 3	S

[a] The sequences of the MFT from several species were aligned with FT-1 from *A. thaliana* and the bovine AAC using the Megalign program from DNAStar.

conserved among MFT orthologues and also contained a high percentage of charged residues (Figure 2A). To test the role of these loop regions in the recruitment of the negatively charged folates to the membrane-penetrating cavity in the transporter, these loops were disrupted by insertion of the short, highly negatively charged c-*myc* peptide (EQKLISEEDL). Two cDNAs encoding MFT proteins with the c-*myc* sequence in intermembrane loop 1 (IM1) or 2 (IM2) were assessed using the cellular glyB complementation assay. The results from this experiment were quite striking. The insertion of the c-*myc* tag into the first intermembrane loop region of the CHO cDNA construct prevented complementation of the glyB cell line, but the addition of the c-*myc* tag to the second intermembrane loop allowed complementation of transfected glyB cells, albeit at somewhat lower frequency than with the N-terminal c-*myc*-tagged CHO MFT cDNA control (Figure 1).

The insertion of the *c-myc* epitope into these intermembrane loops involved insertion of a unique restriction endonuclease site, leading to the addition of two amino acids on each side of the epitope tag. For IM1, these amino acids were proline, which might be expected to disrupt folding of the loops, and arginine, which could partially neutralize the negatively charged nature of the *c-myc* epitope. For IM2, glycine and serine were added, which were less likely to interfere with folding. Since inappropriately folded or inserted membrane proteins are generally targeted for degradation, we assessed the trafficking of the insertional mutants to the mitochondrion using Western blot analysis. Both IM1 and IM2 c-*myc*-tagged MFT proteins were expressed in the mitochondria at levels equivalent to those seen with constructs that complemented the glyB cells, such as N-terminal c-*myc*-CHO *mft* (Figure 2C). We concluded that the inactivity of the c-*myc*-tagged IM1 construct reflected interference with the mechanism of transport, rather than effects on trafficking or protein stability.

Selection of Residues in MFT Structural Domains for Mutagenesis. Several residues within the ORF of the CHO MFT protein were initially selected for mutagenesis based on sequence comparisons across MFT orthologues and paralogues. An alignment of the protein sequences of human, monkey, hamster, mouse, and zebrafish MFT orthologues revealed an overwhelming degree of homology, with the hamster having the highest degree of identity with the mouse MFT (97%) and the least (66%) with the zebrafish protein (*9*). It was of interest to distinguish those structural elements of the MFT protein that are specific to the influx of folates from those common to transport by all MCP family members. Hence, residues were selected that were either completely conserved or had conservative changes in all MFT orthologues but were not conserved in the AAC paralogue (Table 1). However, one of the selected residues, R249, was an exact match to the corresponding residue in the bovine liver AAC (R234) and was central to a motif at the bottom of the internal cavity thought to be involved in the trap-door mechanism of the AAC. One unusual orthologue that was useful in this comparison was the ATF1 protein, an *Arabidopsis thaliana* chloroplast membrane protein that complemented the glyB phenotype at a modest frequency (*28*). The residues used in mammalian, zebrafish, and *Arabidopsis* MFT orthologues and in the human AAC at the positions chosen for mutation are compared in Table 1. Eight of the ten residues were identical across all of the MFT orthologues, and another (R19) had a conservative replacement in one species. Residue 209 was negatively charged (E) in the hamster, but positively charged (K) in human, monkey, and mouse. Six of the ten residues were either identical in the *Arabidopsis* chloroplast protein FT-1 or had conservative replacements.

Subsequent to the initiation of these complementation experiments, crystallographic information became available on the bovine AAC (*17*). Given the sequence homology between the MCP paralogues, we used the AAC structure to thread the sequence of the CHO MFT onto the AAC and used this structure to predict the location of the designed mutations. Of the residues chosen for mutation, six residues (R19, H41, S95, E129, K184, and R249) were within membrane-spanning regions, at least five of which appeared to be facing into the aqueous pore. Three of the mutants (R114, E209, and E219) were located in the intermembrane loop. The last residue mutated (H256) was at the interface between TMD5 and the third matrix-projecting loop and was positively charged.

Alanine Scanning Mutagenesis. All of the mutant constructs were initially studied using the glyB complementation assay (Figure 3A). Because of the two negative charges of the glutamic acid in the folate side chain, it seemed reasonable that the positively charged residues spaced at intervals down the internal aqueous channel of the MFT (see below) would be involved in positioning the folate during its descent into the transport cavity. Remarkably, mutation of the highly conserved residues R19, H41, R114, K184, and H256 to alanine did not significantly alter the comple-

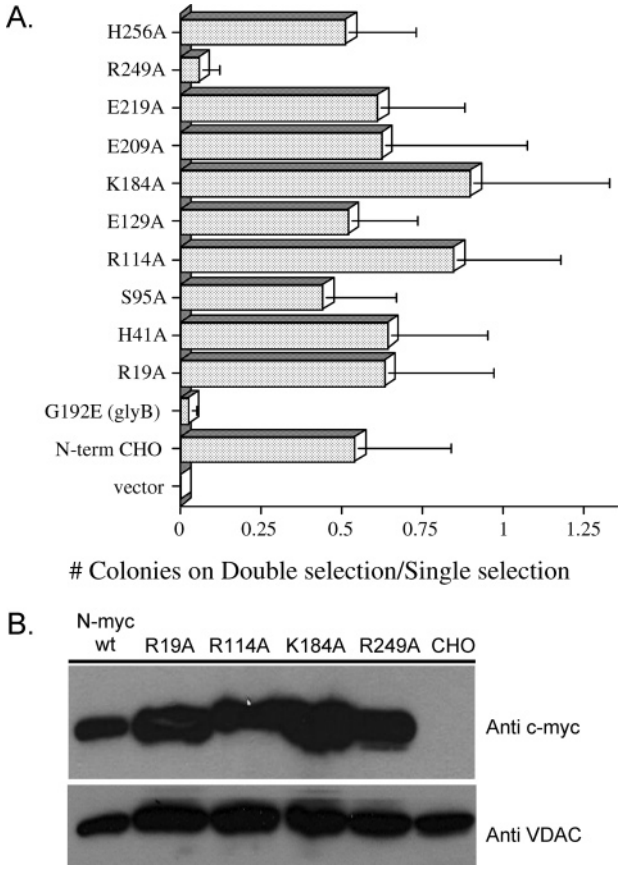

FIGURE 3: The R249A MFT mutant eliminates glyB complementation. (A) Fraction of transfected cells that form colonies in the absence of glycine for stably transfected MFT mutants. The effect of each mutant on cell survival is expressed as a ratio of colonies formed under glycine deprivation versus colonies formed with glycine supplementation. All mutants were constructed using the scaffold of the N-terminal c-*myc*-tagged CHO *mft* cDNA, which is shown as a positive control. For details, see the text. (B) Western blot analysis of the mitochondrial targeting of selected CHO mutants, including the R249A MFT protein. Forty micrograms of mitochondrial protein was analyzed in each well. Mitochondrial proteins from glyB cells stably transfected with the N-terminal c-*myc*-tagged CHO *mft* (N-myc wt) and from untransfected CHO cells (CHO) were used as positive and negative controls, respectively.

mention of the glyB cell line. Likewise, mutation of two highly conserved anionic residues, E129 and E219, did not noticeably disturb function. Mutation of residue 209, which was enigmatically negatively or positively charged in different MFT species but not in paralogues at this position, was also without effect, as was mutation of the highly conserved S95, a residue conservatively modified to T in the AAC. In contrast, transfection of a cDNA for R249A into glyB cells demonstrated no complementation by this mutant MFT species. Western blot analysis revealed no effect of the R249A mutation on the trafficking of the MFT protein to the mitochondria or on protein stability (Figure 3B). The structure (*17*) of the AAC complexed with the transport inhibitor, CATR, revealed that residue R234 of the AAC (the equivalent of MFT R249) held CATR securely in the bottom of the transport basket. We concluded that the charged residues predicted to line the transport cavity of the MFT or the exterior rim of the cavity were surprisingly insensitive to mutagenesis, and none were indispensible to the transit of folates to the transport-triggering binding site. However, the function of residue R249 was central to transport by the MFT.

Transport of Folates into the Mitochondria of Intact Cells. If cells could survive and produce progeny with diminished mitochondrial folate transport, the glyB complementation assay would not be a true indication of the effect of mutations on transport function. To directly estimate the rate of mitochondrial transport of folates, we first followed the time course of uptake of [^{3}H]-5-formyltetrahydrofolate (^{3}H-5-fTHF) into mitochondria in intact CHO cells. The rate of accumulation of ^{3}H-5-fTHF in CHO mitochondria was biphasic, with an initial slope of approximately 6.5×10^{-3} pmol min^{-1} per 10^6 cells over 15−20 min, followed by a slower rate of accumulation at longer times (Figure 4A). These two rates appeared to reflect the rate of initial passage through the inner mitochondrial membrane and the metabolism of folates to polyglutamates in the matrix, respectively. Interestingly, over this time course, the initial mitochondrial uptake rate extrapolated through the origin, and we were not able to detect a time lag associated with accumulation of folates in the cytosolic compartment. The mitochondrial uptake of 5-fTHF in glyB cells was barely detectable and was maximal at the earliest time points studied (Figure 4A). We interpreted the uptake in glyB cells to reflect distribution from the cytosol into the mitochondrial intermembrane space.

The uptake of 5-fTHF into mitochondria of transfected cells was followed over 20 min as an estimate of mitochondrial transport rates. Ten colonies of stable transfectants were selected for each mutant cDNA, and mass cultures of these individual clones were pooled in equal numbers to ensure that transport rates reflected a population of stable transfectants. Although the uptake rates, measured in picomoles per 10^6 cells in 20 min, were lower than in CHO cells for several mutant *mft*s, only the G192E and R249A mutations severely depressed uptake rates (Figure 4B). These experiments involved fractionation of multiple cell pellets with a hand Dounce homogenizer, so that there was some variability of cell breakage with different samples. To normalize for these effects, the mitochondrial uptake data were also expressed as mitochondrial folate content at 20 min as a fraction of total cellular folates (Figure 4B). Surprisingly, most of the point mutations had rather minor effects on mitochondrial initial uptake, although the mutation of some of the residues lining the transport cavity (H41A, S95A, E129A, and K184A) depressed the transport rate by 20−25%. Likewise, H256 depressed the measured uptake by >20%. As with the more variable glyB complementation data (Figure 3), direct mitochondrial uptake estimates led to the conclusion that only the G192E and R249A mutations inactivated the transporter.

Predictions of the Interaction of G192E and R249 from a Homology Model of the MFT Structure. Despite the moderate, although evenly distributed, sequence identity (∼26%) between the hamster MFT protein and the bovine AAC (GenBank accession number P02722), a preliminary assessment of secondary structure conservation using mGenTHREADER demonstrated that the solved AAC (PDB code: 1okc) would be an ideal template for 3D model prediction (*29*, *30*). The 3D model of the MFT predicted by the ESyPred3D server accurately fit the 1okc template with an RMSD of 0.89, and a Sybyl model yielded a nearly indistinguishable fit with a RMSD of 0.84. There was little

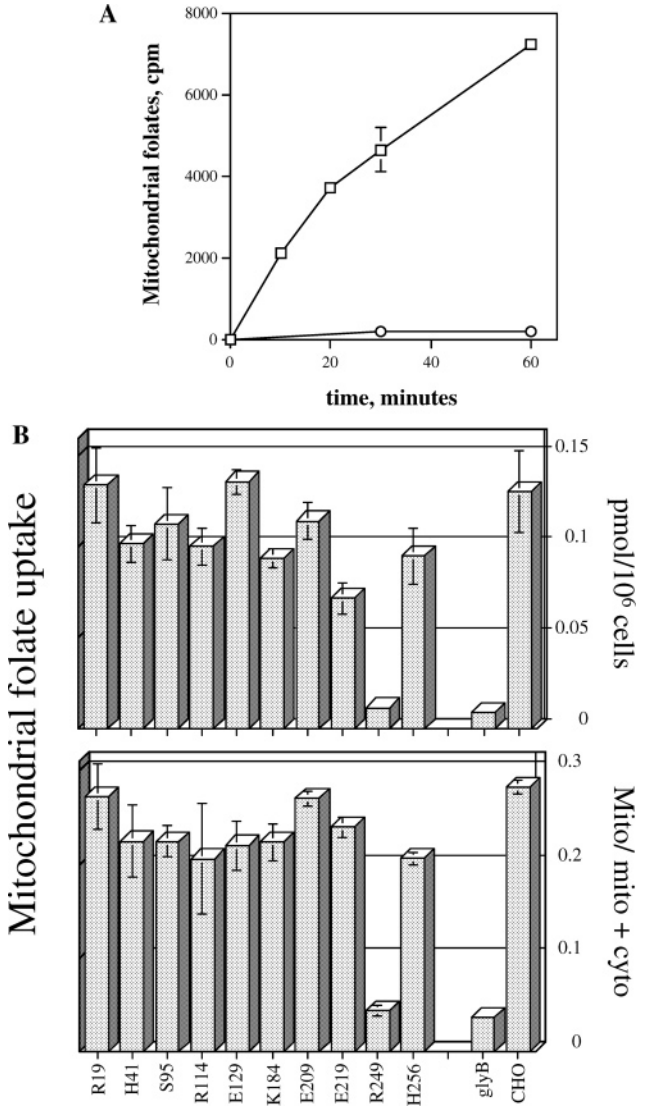

FIGURE 4: Mitochondrial uptake of ^{3}H-5-fTHF. (A) Accumulation of ^{3}H-5-fTHF in mitochondria of CHO cells (open squares) and glyB cells (open circles). Mitochondrial fractions were isolated by Dounce homogenization followed by differential centrifugation, as described in the text. (B) Uptake of ^{3}H-5-fTHF in mitochondria of glyB cells stably transfected with mutant CHO MFT cDNAs. Clones of stable transfectants were incubated with ^{3}H-5-fTHF for 20 min, and the mitochondrial fractions were collected as in (A). The top bar graph shows the level of folates in mitochondria, expressed as picomoles per 10^6 cells, while the bottom graph expresses the data as the ratio of mitochondrial folates to the sum of mitochondrial plus cytosolic folates. Each point represents the mean of two to six experiments, each performed on three replicates ± SD.

deviation in the positions and lengths of helices between the AAC structure and either MFT homology model, while greater deviation was seen in the flexible loops connecting each helix (Figure 5). As seen in the 1okc template, nearly all residues of the MFT model lining the solvent-accessible surface of the cavity were polar, with a good deal of those conserved between the paralogues.

The critical transport residue R249 of the MFT was predicted by this model to occupy the same space as R234 of the bovine AAC. The crystal structure of the bovine AAC suggests (*17*, *31*) that cation−anion interactions between residues D134 and R234, E29 and R137, and D231 and K32 hold together a barrier that prevents entry of ADP into the mitochondrial matrix (Figure 6A). It is thought that substrate recognition induces breakage of these bonds, triggering the three signature peptides to swivel on prolines 27, 132, and 229 and to open a route into the matrix (*31*). Inactivation of the MFT by the R249A mutation is central to understanding the commonality of transport mechanism used by the MFT and the AAC, because the anion−cation interactions typical of the AAC are missing in all MFT orthologues. In fact, the MFT and only four other known mitochondrial transport proteins (encoded by the *flx1*, *yil006w*, *yel006w*, and *rim2* genes in yeast) have a tryptophan at the position analogous to D134 (MFT W142). The residues equivalent to those used by the AAC ion−ion bonds were examined in our homology model. As shown in Figure 6B, the MFT homology model suggests that D44 forms an ion−ion bond with K145, that K47 forms a hydrogen bond with the side chain carbonyl of Q246, and that the side chain of R249 is well positioned to form a π−cation bond with W142. This suggests that those transporters bearing the P(I/L)W motif have evolved a modified mechanism better suited to the chemical composition of their transport substrates. Clearly, the R249A mutation would disrupt this mechanism.

In the functionally null glyB mutant (G192E), the MFT model indicated that E192 would protrude into the cation-lined cavity, surprisingly close to R249 (Figure 6B). As a result, the glyB mutation would permit the formation of a hydrogen bond between R249 and E192 (Figure 6B), stabilizing the side chain of R249 in a conformation not seen in wild-type MFT (Figure 6A). This would decrease the flexibility of R249 needed for opening the barrier to the matrix side of the carrier and would also sterically hinder access to the bottom of the basket. Hence, our studies suggest that the G192E and R249A mutations are both interfering with the function of a π−cation bond central to the mechanism of channel opening.

DISCUSSION

The inner mitochondrial membrane transporter family is quite remarkable: individual family members have diverged sufficiently to allow transport of unique substrates with high specificity, yet the basic mechanism of substrate passage through the membrane is probably common to all family members. One of the best studied members of this protein family, the AAC, transports ADP into the mitochondrial matrix and ATP out. That is, the specificity of a single transport channel protein is different depending upon the direction of movement across the same membrane. It is a continuing question whether an individual transporter molecule facilitates substrate movement in both directions or whether the transporter functions as a dimer, with individual subunits dedicated to one direction of flux. Two key questions about these transporters, at the moment, are the mechanism of membrane penetration by substrate and how evolution has tailored the transport channel to suit individual substrates.

Mitochondrial folate transport is essential to folate metabolism, which is compartmentalized between the mitochondria and the cytosol. Folates are rapidly metabolized to γ-carboxyl-linked polyglutamate forms in the cytosol, and yet indirect but definitive evidence indicates that only folate monoglutamates are substrates for transport into mitochondria (*3*, *8*). This implies competition between cytosolic folylpoly-

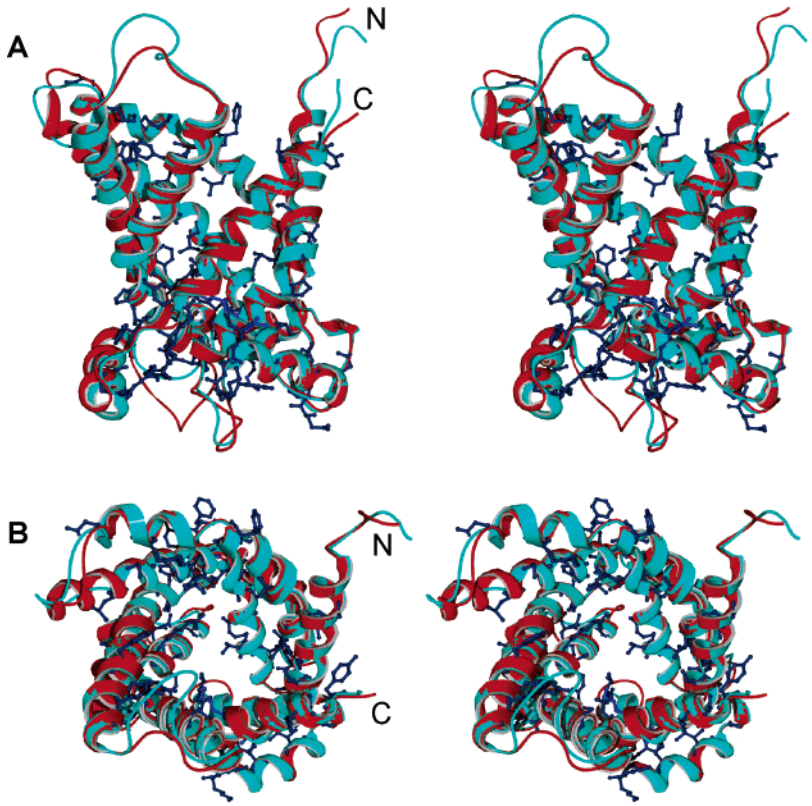

FIGURE 5: Stereo images of the optimized homology model for hamster MFT superimposed on the crystal structure of the bovine AAC. Two views are shown: the top view orients the structures so that the inner mitochondrial membrane would be perpendicular to the plane of the page; in the bottom view, the top structures have been rotated 90 degrees, so that the view is from the intermembrane space down into the transport cavity. The AAC structure is shown in red and the MFT homology model in blue-gray. Residues identical in both sequences are shown as dark blue in ball-and-stick representation. Note that almost all of the identical residues are along the core of the carrier and are spaced throughout the TMDs and that the helix-connecting loops differ between the structures.

glutamate synthetase and the MFT for available folate monoglutamates. It remains an open question whether folates can penetrate back from the mitochondrial matrix into the cytosol, although circumstantial evidence suggests that folylpolyglutamates may efflux back into the cytosol (*7*, *8*, *32*, *33*). Some folate analogues penetrate the mitochondria and potentially cause cytotoxicity at this site, while other antifolates are excluded from the mitochondria (*34*, *35*). How these closely related compounds are distinguished by the MFT is unknown.

Insertional and site-directed mutagenesis was used to probe regions of the MFT protein. Initially, a c-*myc* epitope, EQKLISEEDL, was added to the N- and C-termini and to both intermembrane loops of the CHO MFT protein. In the AAC structure, these peptides line the rim of the cavity facing the intermembrane space. It seemed plausible that the initial recruitment of the negatively charged folate substrate would involve an interaction of substrate with residues located on the intermembrane-facing, outer rim of the MFT. Interestingly, disruption of the first intermembrane loop region completely destroyed the transport function of the MFT protein in our cellular complementation assay, but the other three insertional mutants (N-terminal, C-terminal, and IM2) had little or no effect. In recent studies by Kihira and colleagues (*36*), each residue in the first intermembrane loop of the yeast AAC was individually replaced by a cysteine. Remarkably, while most of these mutations did not affect transport, one mutation at the N-terminus of this intermembrane loop eliminated transport activity and three at the C-terminal portion greatly diminished function. From a series of kinetic and labeling experiments, these authors concluded that charged residues in the N-terminal segment of IM1 were involved in substrate recruitment for subsequent entry into the transport cavity. The effect of insertion of the *myc* peptide might be the result of disruption of the structure of this loop or might be similar to the residue-specific effects seen by Kihira et al. (*36*). However, a defect in mitochondrial targeting of the IM1 construct can be ruled out (Figure 1B), and if the MFT protein with a c-*myc* insertion in IM1 incorrectly inserted into the mitochondrial inner membrane, it would most likely have been targeted for degradation, which was not detected by Western blots (Figure 1B).

Ten amino acids, all well conserved among the MFT paralogues and mostly charged residues, were selected for site-directed mutagenesis. Nine of these mutations had, at most, modest effects on folate uptake. Yet, mutagenesis of the yeast citrate or bovine oxoglutarate carrier at some of the analogous residues had marked effects on function (*37*−*39*), suggesting that the fine details of substrate recognition and positioning in the transport cavity are unique to the individual carriers, presumably reflecting the substrate shape and chemistry. In contrast, the R249A mutant did not retain MFT function, and as a result, cells were unable to survive without an exogenous supply of glycine. When the corresponding residue (R252) in the yeast AAC was mutated to an isoleucine, there was a loss of function (*40*, *41*) similar to what we now report for the hamster MFT. Mutagenesis experiments can now be chosen on the basis of a homology

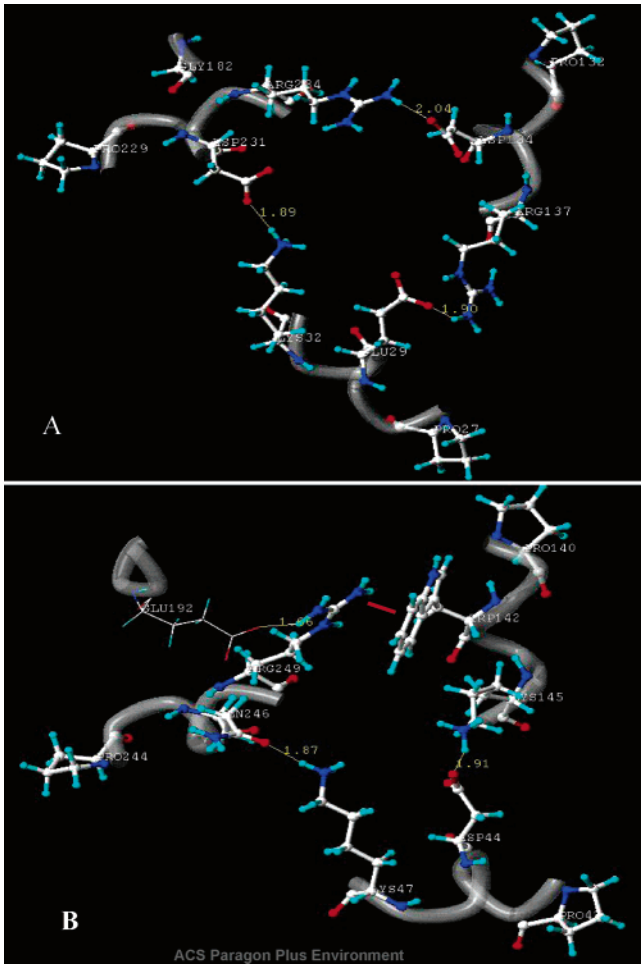

FIGURE 6: Comparison of the peptide components of the proposed trap door of the AAC crystal structure (A) with that of the homology modeled MFT (B). (A) The Px(D/E)xx(K/R) signature sequence of the crystallized AAC (1okc) and residue GLY182 are labeled in white with their three-letter abbreviation and sequence numbers. The α-carbon backbone is shown in light gray ribbon tube display. Predicted salt bridge lengths are shown in yellow with distances in angstroms. Of particular interest is the proximity of Gly182 to Arg234 on TMD5. (B) The predicted structure of the MFT residues equivalent to those shown in (A) for the AAC. Signature sequence residues are identified in white and shown in ball-and-stick representation. Residue 192, as mutated in glyB cells to Glu, is labeled in white and shown in CPK. The α-carbon backbone of the amino acid sequence is shown in white ribbon tube display. Predicted salt/hydrogen bond lengths are shown in yellow, as is the predicted interaction distance between Glu192 and Arg249. Trp142 is also predicted to interact with Arg249 via a π−cation interaction, shown by the red bar. The dual interactions of Arg249 with Glu192 and Trp142 are proposed to be responsible for the inactivity of the glyB MFT; see Discussion.

model for the MFT, which should allow testing of mechanistic hypotheses much more readily.

The predicted secondary structures for the hamster MFT and the bovine AAC were sufficiently similar that a high-quality three-dimensional homology model for the MFT could be constructed on the basis of the crystal structure of the AAC (Figure 5). Several conclusions could be drawn within the constraints of such a homology model. The electrostatic surface potential indicated that the charge distribution surrounding the rim of the homology model varied, with the N-terminus and IM1 electropositive, while the C-terminus and IM2 were electronegative. The residues lining the descent into the transport cavity had an increasingly cationic surface charge. As was seen in the crystal structure of the AAC (*17*), the homology model of the MFT predicted a positively charged floor at the bottom of the transport cavity. However, there are some intriguing differences between the AAC structure and that predicted for the MFT. For instance, the AAC had three tyrosines located on one side of an α-helix and at increasing depth into the aqueous channel; this "tyrosine ladder" is thought to be involved in migration of ADP down into the cavity (*17*, *31*). Such a structure is not apparent in the homology model of the MFT. Also, residue R79 of the AAC is common to all of the AAC paralogues and was proven to be essential to ADP transport by mutagenesis (*40*, *41*); the analogous residue is a glycine in the MFT and all of the yeast P(I/L)W subfamily (*10*) members. These differences make the MFT a particularly interesting member of the MCP family.

One of the distinguishing characteristics of the mammalian MFTs that is maintained in the zebrafish MFT and even in the distant cousin, the AFT1 protein [an *Arabidopsis* chloroplast protein capable of modest complementation of the glyB phenotype (*28*)], is the replacement of the second Px-(D/E) motif with PIW. On the basis of direct structural data (*17*, *31*), this replaced acidic amino acid has been proposed to be involved in one of three ion−ion bonds central to the mechanism of the AAC (Figure 6A), a mechanism thought to be common to most of the MCP members. We now propose that W142 of the hamster MFT, and the equivalent residues of all of the P(I/L)W subfamily members, is involved in a π−cation bond that serves the same function as this ion−ion bond in other MCP members (Figure 6B). Such a π−cation bond was recently used by Robinson and Kunji in their comprehensive modeling studies (*42*). The energetics of a π−cation bond (*43*) appear to be quite favorable to ligand recognition interactions, as judged by the use of this mechanism by the chromodomains of the HP1, CHD1, and polycomb proteins (*44*−*46*) for recognition and docking of N-modified lysines and arginines on the N-terminal tails of histone H3.

A recent detailed model for the substrate binding contacts that align transport substrate in the cavity of the yeast AAC and several related paralogues (*42*) concluded that alignment of ADP in the transport cavity was largely due to three contact points, one of which was defined by G182 and the adjacent isoleucine. This G182 AAC is homologous to G192 in the hamster MFT. Hence, the side chain of the G192E mutation would potentially impose steric hindrance to docking of the incoming MFT substrate. In addition, the proximity of the γ-carboxyl group of the 192E side chain with R249 would allow an ion pair interaction, reinforcing the proposed π−cation bond between R249 and W142 (Figure 6B) and preventing the motion of the R249-containing peptide needed to open the "trap door".

Finally, one has to consider why the MFT and only very few other members of the P(I/L)W subfamily have evolved to replace a D or E with a W. It is noted that the *flx1* protein transports FAD, the *rim2p* transporter accepts pyrimidine nucleotides into and out of the mitochondria, and the substrate for the *yil006w* transporter is NAD^+ (*47*−*49*). The substrate for the *yel006w* protein is still undefined. Thus, the P(I/L)W subfamily members whose function has been assigned have evolved to transport substrates with aromatic ring systems. We would postulate that the aromatic rings of

the substrates of these transporters break the proposed π−cation bond by interacting directly with the central W residue. This mechanism does not explain all of the data, for instance, why the ATP/ADP exchanger does not use a PIW motif, but it suggests a number of testable hypotheses that are currently under direct investigation.

ACKNOWLEDGMENT

We thank Steve Titus and Professor Glen Kellogg for critiques of the manuscript.

REFERENCES

1. Cook, R. J., and Blair, J. A. (1979) The distribution and chemical nature of radioactive folates in rat liver cells and rat liver mitochondria, *Biochem. J. 178*, 651−659.
2. Corrocher, R., and Hoffbrand, A. V. (1972) Subcellular localization of folate and effect of methotrexate on the incorporation of radioactive folic acid into guinea-pig liver folate, *Clin. Sci. 43*, 812−822.
3. Lin, B. F., Huang, R. F., and Shane, B. (1993) Regulation of folate and one-carbon metabolism in mammalian cells. III. Role of mitochondrial folylpoly-γ-glutamate synthetase, *J. Biol. Chem. 268*, 21674−21679.
4. Sankar, D. V., Geisler, A., and Rozsa, P. W. (1969) Intracellular distribution of folic acid in mouse liver, *Experientia 25*, 691−692.
5. Shin, Y. S., Chan, C., Vidal, A. J., Brody, T., and Stokstad, E. L. (1976) Subcellular localization of gamma-glutamyl carboxypeptidase and of folates, *Biochim. Biophys. Acta 444*, 794−801.
6. Appling, D. R. (1991) Compartmentation of folate-mediated one-carbon metabolism in eukaryotes, *FASEB J. 5*, 245−251.
7. Titus, S. A., and Moran, R. G. (2000) Retrovirally mediated complementation of the glyB phenotype. Cloning of a human gene encoding the carrier for entry of folates into mitochondria, *J. Biol. Chem. 275*, 36811−36817.
8. Freemantle, S. J., Taylor, S. M., Krystal, G., and Moran, R. G. (1995) Upstream organization of and multiple transcripts from the human folylpoly-γ-glutamate synthetase gene, *J. Biol. Chem. 270*, 9579−9584.
9. McCarthy, E. A., Titus, S. A., Taylor, S. M., Jackson-Cook, C., and Moran, R. G. (2004) A mutation inactivating the mitochondrial inner membrane folate transporter creates a glycine requirement for survival of chinese hamster cells, *J. Biol. Chem. 279*, 33829−33836.
10. Nelson, D. R., Felix, C. M., and Swanson, J. M. (1998) Highly conserved charge-pair networks in the mitochondrial carrier family, *J. Mol. Biol. 277*, 285−308.
11. Wohlrab, H. (2005) The human mitochondrial transport protein family: identification and protein regions significant for transport function and substrate specificity, *Biochim. Biophys. Acta 1709*, 157−168.
12. Saraste, M., and Walker, J. E. (1982) Internal sequence repeats and the path of polypeptide in mitochondrial ADP/ATP translocase, *FEBS Lett. 144*, 250−254.
13. Capobianco, L., Bisaccia, F., Michel, A., Sluse, F. E., and Palmieri, F. (1995) The N- and C-termini of the tricarboxylate carrier are exposed to the cytoplasmic side of the inner mitochondrial membrane, *FEBS Lett. 357*, 297−300.
14. Ferreira, G. C., Pratt, R. D., and Pedersen, P. L. (1990) Mitochondrial proton/phosphate transporter. An antibody directed against the COOH terminus and proteolytic cleavage experiments provides new insights about its membrane topology, *J. Biol. Chem. 265*, 21202−21206.
15. Capobianco, L., Brandolin, G., and Palmieri F. (1991) Transmembrane topography of the mitochondrial phosphate carrier explored by peptide-specific antibodies and enzymatic digestion, *Biochemistry 30*, 4963−4969.
16. Walker, J. E., and Runswick, M. J. (1993) The mitochondrial transport protein superfamily, *J. Bioenerg. Biomembr. 25*, 435−446.
17. Pebay-Peyroula, E., Dahout-Gonzalez, C., Kahn, R., Trezeguet, V., Lauquin, G. J., and Brandolin, G. (2003) Structure of mitochondrial ADP/ATP carrier in complex with carboxyatractyloside, *Nature 426*, 39−44.
18. Chasin, L. A., Feldman, A., Konstam, M., and Urlaub, G. (1974) Reversion of a Chinese hamster cell auxotrophic mutant, *Proc. Natl. Acad. Sci. U.S.A. 71*, 718−722.
19. Kao, F., Chasin, L., and Puck, T. T. (1969) Genetics of somatic mammalian cells. X. Complementation analysis of glycine-requiring mutants, *Proc. Natl. Acad. Sci. U.S.A. 64*, 1284−1291.
20. Sanbrook, J., and Russell, D. W. (2001) *Molecular Cloning. A Laboratory Manual*, 3rd ed., sect. 13.36, Cold Spring Harbor Press, Cold Spring Harbor, NY.
21. Lambert, C., Leonard, N., De Bolle, X., and Depiereux, E. (2002) ESyPred3D: Prediction of proteins 3D structures, *Bioinformatics 18*, 1250−1256.
22. Guex, N., and Peitsch, M. C. (1997) SWISS-MODEL and the Swiss-PdbViewer: an environment for comparative protein modeling, *Electrophoresis 18*, 2714−2723.
23. Luthy, R., Bowie, J. U., and Eisenberg, D. (1992) Assessment of protein models with three-dimensional profiles, *Nature 356*, 83−85.
24. Sippl, M. J. (1993) Recognition of errors in three-dimensional structures of proteins, *Proteins 17*, 355−362.
25. Canutescu, A. A., Shelenkov, A. A., and Dunbrack, R. L. Jr. (2001) A graph-theory algorithm for rapid protein side-chain prediction, *Protein Sci. 12*, 2001−2014.
26. Taylor, R. T., and Hanna, M. L. (1982) Folate-dependent enzymes in cultured Chinese hamster ovary cells: impaired mitochondrial serine hydroxymethyltransferase activity in two additional glycine-auxotroph complementation classes, *Arch. Biochem. Biophys. 217*, 609−623.
27. Colombini, M. (1983) Purification of VDAC (voltage-dependent anion-selective channel) from rat liver mitochondria, *J. Membr. Biol. 74*, 115−121.
28. Bedhomme, M., Hoffmann, M., McCarthy, E. A., Gambonnet, B., Moran, R. G., Rebeille, F., and Ravanel, S. (2005) Folate metabolism in plants: an *Arabidopsis* homolog of the mammalian mitochondrial folate transporter mediates folate import into chloroplasts, *J. Biol. Chem. 280*, 34823−34831.
29. Jones, D. T. (1999) GenTHREADER: an efficient and reliable protein fold recognition method for genomic sequences, *J. Mol. Biol. 287*, 797−815.
30. McGuffin, L. J., and Jones, D. T. (2003) Improvement of the GenTHREADER method for genomic fold recognition, *Bioinformatics 19*, 874−81.
31. Pebay-Peyroula, E., and Brandolin, G. (2004) Nucleotide exchange in mitochondria: insight at a molecular level, *Curr. Opin. Struct. Biol. 14*, 420−425.
32. Lin, B.-F., and Shane, B. (1994) Expression of *Escherichia coli* folylpolyglutamate synthetase in the Chinese hamster ovary cell mitochondria, *J. Biol. Chem. 269*, 9705−9713.
33. Qi, H., Atkinson, I., Xiao, S., Choi, Y.-J., Tobimatsu, T., and Shane, B. (1999) Folylpoly-γ-glutamate synthetase: generation of isozymes and the role in one carbon metabolism and antifolate cytotoxicity, *Adv. Enzyme Regul. 39*, 263−273.
34. Kim, J. S., and Shane, B. (1994) Role of folylpolyglutamate synthetase in the metabolism and cytotoxicity of 5-deazaacyclotetrahydrofolate, an anti-purine drug, *J. Biol. Chem. 269*, 9714−9720.
35. Kim, J. S., Lowe, K. E., and Shane, B. (1993) Regulation of folate and one-carbon metabolism in mammalian cells. IV. Role of folylpoly-γ-glutamate synthetase in methotrexate metabolism and cytotoxicity, *J. Biol. Chem. 268*, 21680−21685.
36. Kihira, Y., Majima, E., Shinohara, Y, and Terada, H. (2005) Cysteine labeling studies detect conformational changes in region 106−132 of the mitochondrial ADP/ATP carrier of *Saccharomyces cerevisiae*, *Biochemistry 44*, 184−192.
37. Ma, C., Kotaria, R., Major, J. A., Remani, S., Walters, D. E., and Kaplan, R. S. (2005) The yeast mitochonrial citrate transport protein. Characterization of transmembrane domain III residue involved in substrate translocation, *J. Biol. Chem. 280*, 2331−2340.
38. Cappello, A. R., Curcio, R., Miniero, D. V., Stipani, I., Robinson, A. J., Kunji, E. R. S., and Palmieri, F. (2006) Functional and structural role of amino acid residues in the even numbered transmembrane α-helices of the bovine mitochondrial oxoglutarate carrier, *J. Mol. Biol. 363*, 51−62.
39. Stipani, V., Cappello, A. R., Daddabbo, L., Natuzzi, D., Miniero, D. V., Stipani, I., and Palmieri, F. (2001) The mitochondrial oxoglutarate carrier: Cysteine-scanning mutagenesis of transmem-

brane domain IV and sensitivity of Cys mutants to sulfhydral reagents, *Biochemistry 40*, 15805−15810.
40. Heidkämper, D., Müller, V., Nelson, D. R., and Klingenberg, M. (1996) Probing the role of positive residues in the ADP/ATP carrier from yeast. The effect of six arginine mutations on transport and the four ATP versus ADP exchange modes, *Biochemistry 35*, 16144−16152.
41. Nelson, D. R., Lawson, J. E., Klingenberg, M., and Douglas, M. G. (1993) Site-directed mutagenesis of the yeast motochondrial ADP/ATP translocator. Six arginines and one lysine are essential, *J. Mol. Biol. 230*, 1159−1170.
42. Robinson, A. J., and Kunji, E. R. S. (2006) Mitochondrial carriers in the cytoplasmic state have a common substrate binding site, *Proc Natl. Acad. Sci. U.S.A. 106*, 2617−2622.
43. Dougherty, D. A. (1996) Cation interactions in chemistry and biology: A new view of benzene, Phe, Tyr, and Trp, *Science 271*, 163−168.
44. Flanagan, J. F., Mi, L.-Z., Chruszcz, M., Cymborowski, M., Clines, K. L., Kim, Y., Minor, W., Rastinejad, F., and Khorasanizadeh, S. (2005) Double chromodomains cooperate to recognize the methylated histone H3 tail, *Nature 438*, 1181−1185.
45. Min, Y., Zhang, Y., and Xu, R.-M. (2003) Structural basis for specific binding of polycomb chromodomain to histone H3 methylated at Lys 27, *Genes Dev. 17*, 1823−1828.
46. Nielsen, P. R., Nietlispach, D., Mott, H. R., Callaghan, J., Bannister, A., Kouzarides, T., Murzin, A. G., Murzina, N. V., and Laue, E. D. (2002) Structure of the HP1 chromodomain bound to histone H3 methylated at lysine 9, *Nature 416*, 103−107.
47. Tzagoloff, A., Jang, J., Glerum, D. M., and Wu, M. (1996) FLX1 codes for a carrier protein involved in maintaining a proper balance of flavin nucleotides in yeast mitochondria, *J. Biol. Chem. 271*, 7392−7397.
48. Marobbio, C. M., Di Noia, M. A., and Palmieri, F. (2006) Identification of a mitochondrial transporter for pyrimidine nucleotides in *Saccharomyces cerevisiae*: Bacterial expression, reconstitution and functional characterization, *Biochem. J. 393*, 441−446.
49. Todisco, S., Agrimi, G., Castegna, A., and Palmieri, F. (2006) Identification of the mitochondrial NAD^+ transporter in *Saccharomyces cerevisiae*, *J. Biol. Chem. 281*, 1524−1531.

BI062191+